First Comparisons of Surface Temperature Estimations between ECOSTRESS, ASTER and Landsat 8 over Italian Volcanic and Geothermal Areas

Malvina Silvestri [1,2,]* , **Vito Romaniello [1]**, **Simon Hook [3]**, **Massimo Musacchio [1]**, **Sergio Teggi [2]** and **Maria Fabrizia Buongiorno [1]**

[1] Istituto Nazionale di Geofisica e Vulcanologia, Osservatorio Nazionale Terremoti, Via di Vigna Murata 605, 00143 Roma, Italy; vito.romaniello@ingv.it (V.R.); massimo.musacchio@ingv.it (M.M.); fabrizia.buongiorno@ingv.it (M.F.B.)

[2] Department of Engineering "Enzo Ferrari", University of Modena and Reggio Emilia, Via Vivarelli 10, 41125 Modena, Italy; sergio.teggi@unimore.it

[3] California Institute of Technology Jet Propulsion Laboratory, Pasadena, CA 91109, USA; simon.hook@jpl.nasa.gov

* Correspondence: malvina.silvestri@ingv.it; Tel.: +39-06-51860-732

Abstract: The ECO System Spaceborne Thermal Radiometer Experiment on Space Station (ECOSTRESS) is a new space mission developed by NASA-JPL which launched on July 2018. It includes a multispectral thermal infrared radiometer that measures the radiances in five spectral channels between 8 and 12 μm. The primary goal of the mission is to study how plants use water by measuring their temperature from the vantage point of the International Space Station. However, as ECOSTRESS retrieves the surface temperature, the data can be used to measure other heat-related phenomena, such as heat waves, volcanic eruptions, and fires. We have cross-compared the temperatures obtained by ECOSTRESS, the Advanced Spaceborne Thermal Emission and Reflectance radiometer (ASTER) and the Landsat 8 Thermal InfraRed Sensor (TIRS) in areas where thermal anomalies are present. The use of ECOSTRESS for temperature analysis as well as ASTER and Landsat 8 offers the possibility of expanding the availability of satellite thermal data with very high spatial and temporal resolutions. The Temperature and Emissivity Separation (TES) algorithm was used to retrieve surface temperatures from the ECOSTRESS and ASTER data, while the single-channel algorithm was used to retrieve surface temperatures from the Landsat 8 data. Atmospheric effects in the data were removed using the moderate resolution atmospheric transmission (MODTRAN) radiative transfer model driven with vertical atmospheric profiles collected by the University of Wyoming. The test sites used in this study are the active Italian volcanoes and the Parco delle Biancane geothermal area (Italy). In order to test and quantify the difference between the temperatures retrieved by the three spaceborne sensors, a set of coincident imagery was acquired and used for cross comparison. Preliminary statistical analyses show a very good agreement in terms of correlation and mean values among sensors over the test areas.

Keywords: ECOSTRESS; Landsat 8; ASTER; surface temperature estimation

1. Introduction

The estimation of land surface temperature (LST) using Thermal InfraRed (TIR) remote sensing data is a well-developed method offering a quick way to estimate reliable parameters of land surface physical processes on different scales with a positive cost–benefit ratio. The use of satellites offers the possibility of acquiring data in difficult or dangerous to access areas. Moreover, TIR satellite imagery

highlights the main surface changes which are potentially related to underground energy sources that could be risks to health and human activities. The study areas chosen for this work (Figure 1) are the main active Italian volcanoes: Mt. Etna (Etn), Vesuvio (Ves), Solfatara (Sol), Stromboli (Str), and Vulcano (Vul). Moreover, a geothermal test site, the Parco delle Biancane (PdB) area in Tuscany, was selected in order to analyze the capability of satellite data to detect thermal anomalies in non-volcanic areas. All selected areas are characterized by high-temperature geothermal energy sources, commonly marked by thermal manifestations such as fumaroles, steaming ground, hot springs, volcanic gas vents, craters, and mud pools [1–4]. These areas must be commonly subjected to geophysical monitoring where measurements of shallow and surface temperatures may play an important role in the field of thermal monitoring. Anomalies in thermal flux correlated with gas emissions and surface deformation could be, for example, precursory to changes in the state of volcano activity, such as impending eruption [5]. Surface thermal signatures may also be used to define the development of shallow structures present at both volcanic and geothermal areas and possibly related to tectonic activity along active faults.

Figure 1. Areas of interest in Italy (Photo credits: Google Earth, M. Silvestri and M. Musacchio).

Remote sensing represents an effective and expeditious tool for acquiring infrared images over large areas affected by thermal anomalies. Most Earth-observing satellites pass over an area at the same time of day (Sun-synchronous orbit), measuring targets with the same illumination conditions. Unfortunately, the sensors acquiring data in the TIR range that have frequent revisit time (every day) have a low spatial resolution (1 km or more). Sensors with a longer revisit time (16 days) have a medium-high spatial resolution (90–100 m). TIR data with low spatial resolution [6] do not allow the detection of thermal anomalies in areas on the order of hundreds of meters, while data with a low temporal resolution are inadequate for real-time monitoring due to the transitory nature of many volcanic processes. Until recently, there were only two types of satellite data which were suitable for estimating LST at medium-high spatial resolution: the Advanced Spaceborne Thermal Emission and Reflection Radiometer (ASTER) and TIRS on Landsat 8 (L8). The new space mission ECOSTRESS on board the International Space Station has shorter revisit times and higher spatial resolution (39×68 m) than ASTER and L8.

The aim of this study was to cross-compare LST estimates from ASTER, L8 and ECOSTRESS-retrieved LST, based on the radiance, using well-known procedures, to evaluate the reliability of the results for future geophysical studies.

2. Satellite Data and Methods

2.1. Satellite Data: ASTER, Landsat 8 and ECOSTRESS

ASTER, launched on December 1999 and still in operation, is mainly used to study surface temperature and emissivity with a relatively high spatial resolution. ASTER measures radiance in the Visible and Near-InfraRed (VNIR, 0.52 to 0.86 μm) and TIR range (8.12 to 11.65 μm) with a pixel size of 15 m and 90 m, respectively [7,8], and a revisit time of 16 days. ASTER also measured radiance in Short-Wave InfraRed (SWIR, 1.6 to 2.43 μm) spectral range with a 30 m spatial resolution, but the SWIR sensor is no longer functioning as of April 2008.

L8 is the most recent satellite of NASA Landsat program, which is the longest continuous mission for the collection of Earth Observation (EO) data. Launched on February 2013 [9,10], L8's payload consists of two sensors: the OLI (Operational Land Imager) and the TIRS (Thermal InfraRed Sensor). The two thermal TIRS bands (see Table 1) enable the retrieval of surface temperature after the removal of atmospheric effects. In this work, only the band at 10.9 μm (B_{10}) is used, taking into account the known calibration problems of the band at 12.0 μm (B_{11}) in the dual thermal bands of L8 [9,11]. Like ASTER, the revisit time of L8 is 16 days.

Table 1. Sensor technical characteristics and thermal bands used for this work. [1] Bands not available after 15 May, 2019. ECOSTRESS: ECO System Spaceborne Thermal Radiometer Experiment on Space Station; ASTER: Advanced Spaceborne Thermal Emission and Reflectance radiometer; TIRS: Thermal Infrared Sensor; FWHM: Full Width at Half Maximum.

Description	ECOSTRESS	ASTER	TIRS-L8	Unit
Number of thermal spectral bands	5	5	2	-
Measured band centers	8.29 [1]; 8.78; 9.20 [1]; 10.49; 12.09	8.29; 8.63; 9.07; 10.66; 11.32	10.90; 12.00	μm
Measured FWHM per band	0.35; 0.31; 0.39; 0.41; 0.61	0.35; 0.35; 0.35; 0.70; 0.70	0.60; 1.00	μm
Pixel size at nadir	69 × 38	90	100	m
Swath width	384	60	185	Km
Revisit time	~4–5	16	16	Days

ECOSTRESS is the new space mission of NASA-JPL which launched on July 2018, with a multispectral thermal infrared radiometer to measure radiance in five spectral channels ranging from 8 to 12 μm and an additional band at 1.6 μm for geolocation and cloud detection (six bands in total) [12–14]. ECOSTRESS has been launched with the aim of measuring the temperature of plants and understanding their evaporative stress [14]. Its high spatial (69 × 38 meters; 2 pixels in cross track and 1 pixel in down track) and revisit time (about 4–5 days) provides a significant improvement on the operative thermal infrared missions for LST estimation.

Table 1 shows the technical features of the satellite sensors used.

Table 2 summarizes the satellite dataset used in the present study considering the same period and the same areas shown in Figure 1 for the comparison between ECOSTRESS and L8. Unfortunately, the search of ASTER images to compare with ECOSTRESS images for the same areas has produced only one image (listed in Table 3).

In order to retrieve the LST, the Top Of Atmosphere (TOA) radiance L1T data (Terrain corrected level) was used for ASTER and L8, while for ECOSTRESS, the resampled radiance L1B [15] was used. After 15 May 2019, ECOSTRESS data were acquired only for three bands: 8.78 μm, 10.49 μm, and 12.09 μm. The 8.29 μm and 9.20 μm bands are filled with dummy values to accommodate the direct streaming of data from the ISS, as reported in the Known Issues section on their website [15].

Table 2. ECOSTRESS and L8 data for the same time and close in time.

Date	Area	ECOSTRESS Time (UTC)	TIRS-L8 Time (UTC)
20 September 2018	PdB	20:11	20:53
27 February 2019	Sol	10:15	09:47
27 February 2019	Ves	10:15	09:47
14 July 2019	Etn	21:10	20:46
14 July 2019	Str	21:10	20:46
14 July 2019	Vul	21:10	20:46

Table 3. ECOSTRESS and ASTER data close in time.

Date	Area	ECOSTRESS Time (UTC)	ASTER Time (UTC)
13 July 2019	Sol	22:00	21:10

2.2. Methodology for LST Estimation

To retrieve LST, two different methods have been used for ASTER–ECOSTRESS and L8, respectively. Both methods require the atmospheric correction terms to be obtained by using the moderate resolution atmospheric transmission (MODTRAN) code [16] and the atmospheric sounding data collected by the University of Wyoming (in terms of temperature, humidity, and the pressure of the atmospheric profile) and referred to the sounding site nearest to the studied areas [17].

The Temperature and Emissivity Separation (TES) algorithm has been considered for ASTER and estimates surface temperature and spectral emissivity images for multi and hyperspectral satellite images [18–24] using at least three thermal bands; for this reason, this methodology is typically used for ASTER and can be suitable also for ECOSTRESS, as both have five TIR channels in the same spectral range.

The TES method cannot be applied to TIRS-L8 thermal data due to the presence of only two bands in the TIR range; thus, for this analysis, we have used a single-channel methodology which was already tested in [2,24] for retrieving LST. For TIRS–L8 data, the effects of surface emissivity are corrected using the ASTER 05 Emissivity product.

2.3. Methodology of Comparison

The goodness of fit between temperature estimates from the different sensors is evaluated by using several statistical parameters. In particular, the Pearson correlation coefficient is used to evaluate the correlation between the temperature estimates, and the absolute bias and the root mean square error (RMSE) are also calculated to evaluate the average differences and the spread of the compared datasets.

$$Bias = \sum_{i=1}^{N} (T_{Ei} - T_{Si})/N, \tag{1}$$

$$RMSE = \sqrt{(\sum_{I=1}^{N} (T_{Ei} - T_{Si})^2)/N}, \tag{2}$$

where T_{Ei} is the temperature estimated by means of ECOSTRESS data for the i-th pixel; T_{Si} is the same for L8 or ASTER, respectively.

In order to compare the LSTs retrieved by the three sensors, which have different pixel spatial resolutions, all LSTs were resampled to 90 meters of spatial resolution using the nearest neighbor (NN) resampling method implemented in the Environment for Visualizing Images (ENVI) software. The

re-sampled ECOSTRESS LST estimates were compared pixel by pixel with corresponding LST values from ASTER and L8 for acquisitions that were close in time.

3. Results

Figure 2 shows the maps of surface temperature estimates as derived from ECOSTRESS and L8 data, respectively, at PdB, Sol, Ves, Str, Vul and Etn; in Figure 3, the comparison at the Solfatara test (Sol) site of ECOSTRESS and ASTER products is shown.
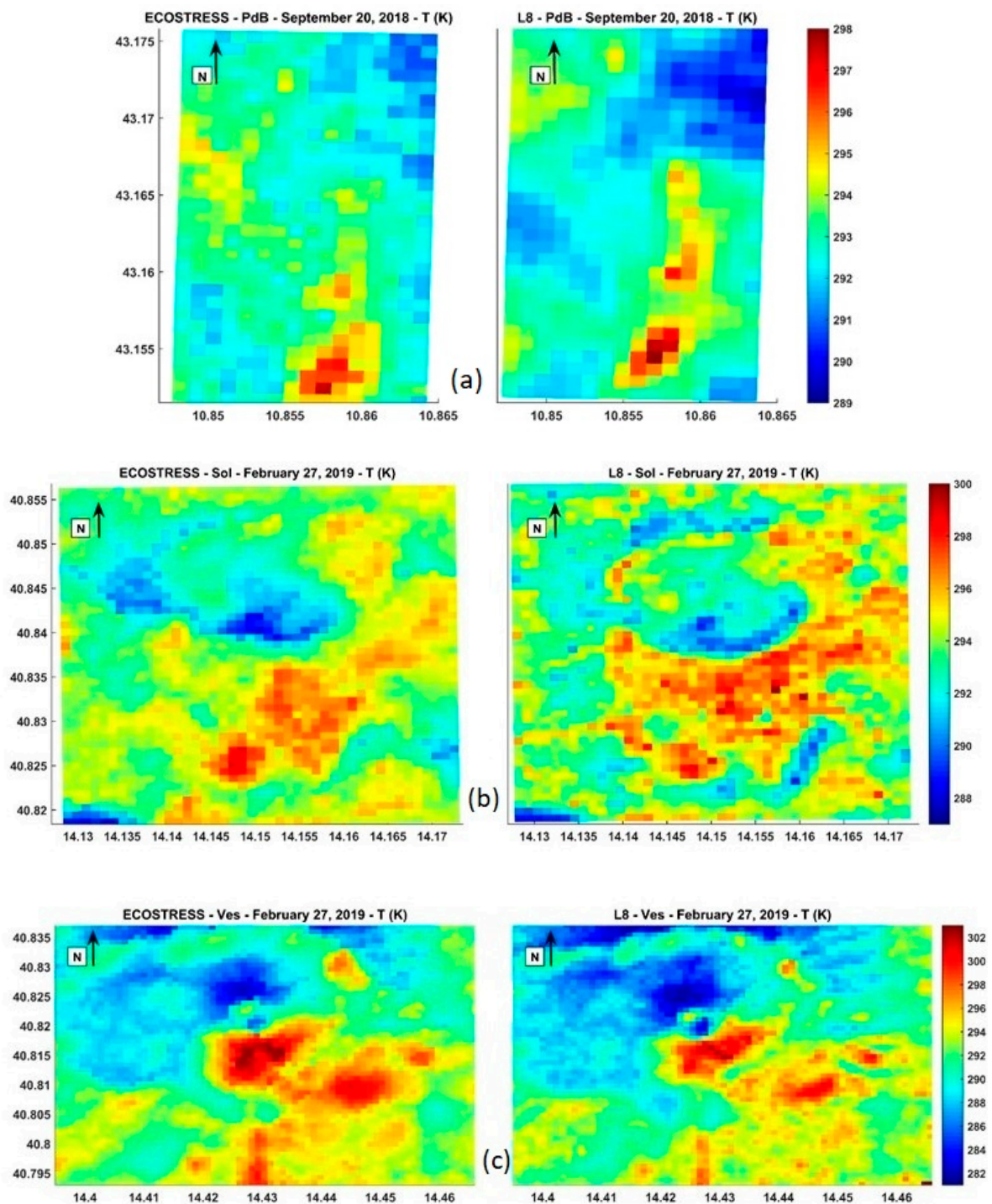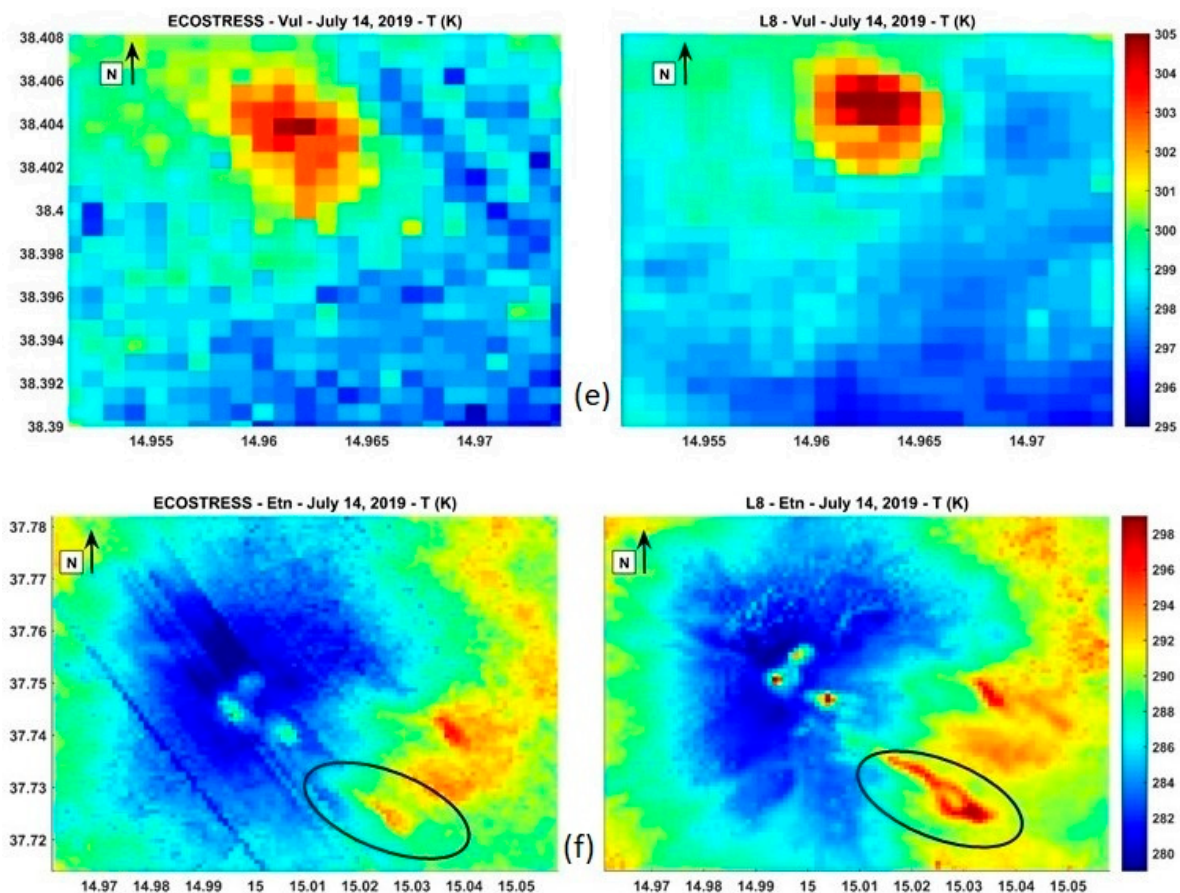

Figure 2. *Cont.*

Figure 2. Surface temperature estimates by ECOSTRESS (**left**) and L8 data (**right**) at Parco delle Biancane (**a**), Solfatara (**b**), Vesuvio (**c**), Stromboli (**d**), Vulcano (**e**), Etna (**f**). North is aligned with the vertical axis and the pixel size is 90 m. In the oval, the lava flow which occurred during the eruption is highlighted.
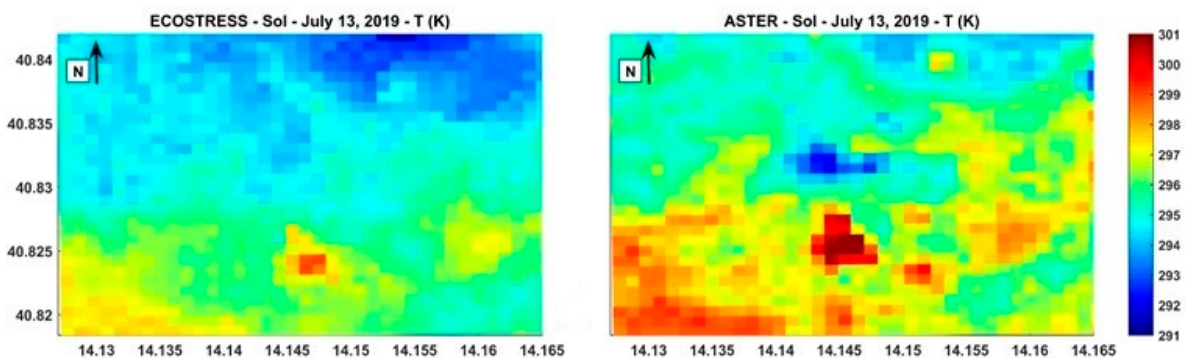

Figure 3. Surface temperature estimates of ECOSTRESS (**left**) and ASTER data (**right**) on Solfatara site. North is aligned with the vertical axis and the pixel size is 90 m.

The main features of the derived thermal fields are in general very similar for both sensors. In Figure 2a, the Parco delle Biancane is characterized by steam and gas emanations and an intense alteration of outcrops and areas where thermal anomalies are present. Similar comparisons are seen for the volcano areas in Figure 2. In Figure 2d, the data show the active portions of the lava flow for the Stromboli volcano during the last eruption on 3 July increased on the evening of 12 July [25]. The ECOSTRESS acquisition for the Mt. Etna area (Figure 2f) seems to have some problems in that it does not allow the detection of the lava flow that erupted in the night of 29–30 May 2019 [26] and

which was still present on 14 July. Moreover, the stripe appearing in Figure 2f for ECOSTRESS is due to the apparent spatial geolocation discrepancies [27].

The temperature estimates are quantitatively compared pixel by pixel for each image pairs and the statistical parameters described in Section 2.3 are calculated. Scatter plots of the cross-comparisons are reported in Figures 4 and 5.
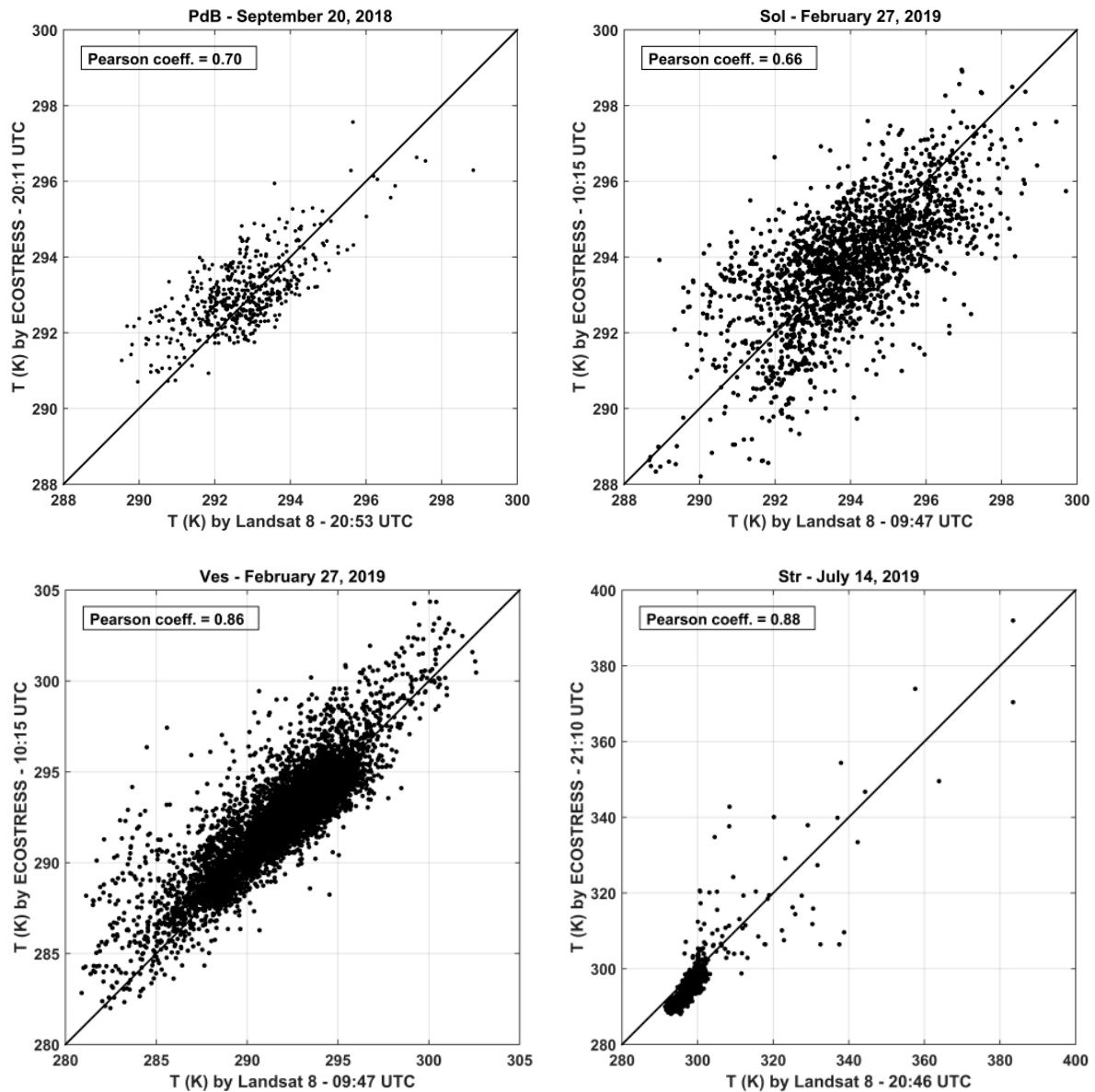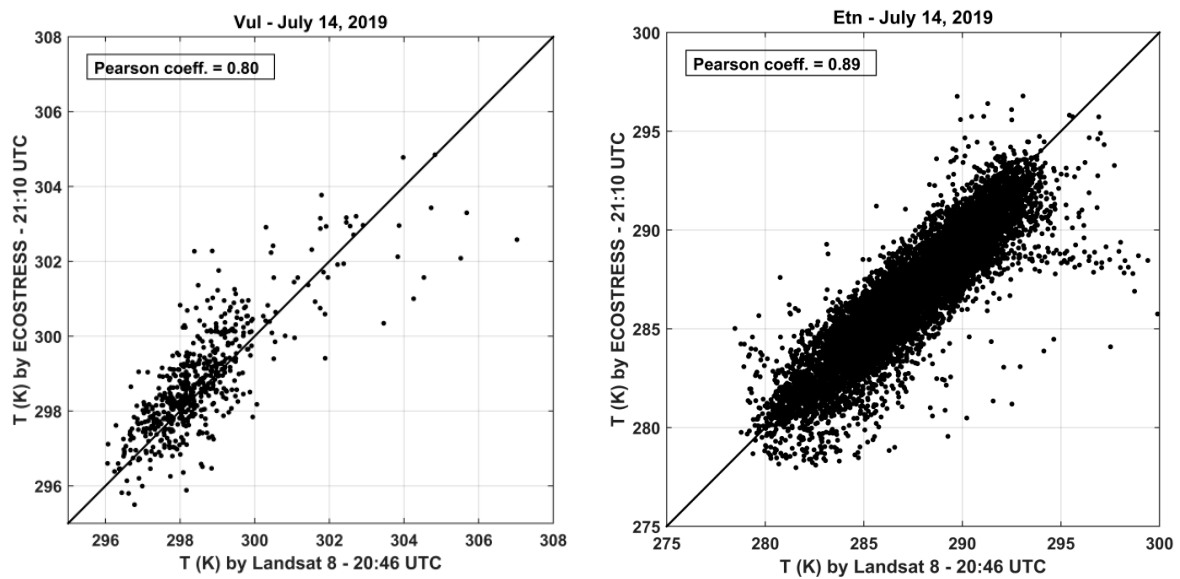

Figure 4. *Cont.*

Figure 4. Scatter plots for comparison of LST–ECOSTRESS vs. L8. The black line is the bisector.
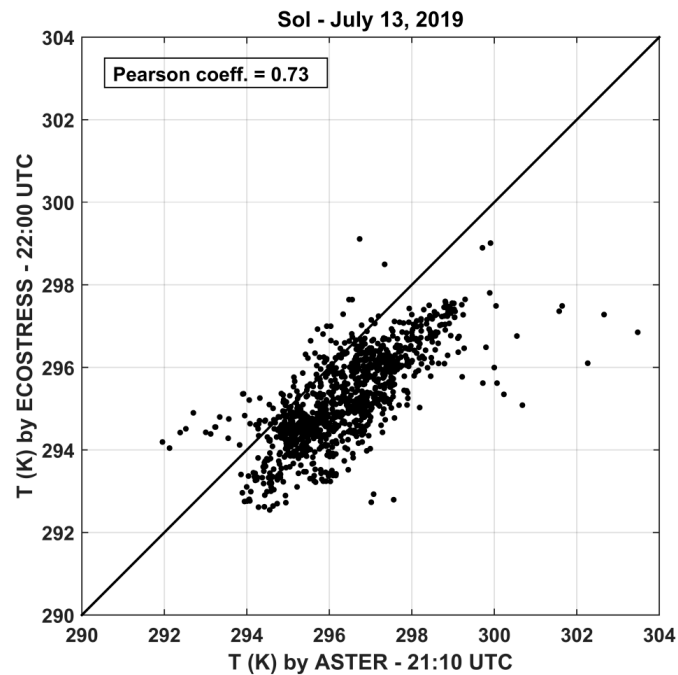

Figure 5. Comparison of LST–ECOSTRESS vs. ASTER. The black line is the bisector.

The resulting values of the Pearson coefficient, bias, and RMSE computed for each pair of images are reported in Table 4.

Table 4. Results of statistical analysis. RMSE: root mean square error. Positive and negative values of Bias represent ECOSTRESS overestimation and underestimation, respectively.

Area and Date	Pearson Coefficient	Bias (K)	RMSE (K)
PdB; 20 September 2018	0.70	+0.31	0.93
Sol; 27 February 2019	0.66	−0.17	1.36
Ves; 27 February 2019	0.86	+0.63	1.75
Etn; 14 July 2019	0.89	−0.73	1.72
Str; 14 July 2019	0.88	−2.47	4.17
Vul; 14 July 2019	0.80	+0.26	0.93
Sol; 13 July 2019 (ASTER)	0.73	−1.13	1.46

4. Discussion

In this work, we compare the LSTs obtained by different sensors on the same day and at approximately the same time. The differences in the acquisition time vary from 30 up to 50 min. Despite the aim of this work, it is important to emphasize that monitoring activity with satellites can be improved by having more than one measurement per day. Stressing this approach, geostationary sensors provide hundreds of images per day but with a very coarse spatial resolution, which is not really useful for monitoring purposes. Indeed, the contribution made by medium-high spatial resolution sensors with a low revisit time should be noted.

Concerning the spatial resolution in this work, the homogenization of ground spatial distance (GSD) has been deployed in order to cross-compare the results derived by the processing. The 90 m pixel resolution resizing has been considered due to the alignment of the dataset to the standard data delivered by ASTER, using this as a landmark. All satellite data used for the retrieval of temperature have been re-sampled by using the NN method to obtain a homogeneous dataset in terms of GSD. This resampling method is suitable for resampling categorized data and for non-linear features as thermal anomalies appear.

In order to implement the direct streaming option of ECOSTRESS, NASA decided that their new acquisition approach after 15 May 2019 would be to only download TIR data for bands 2, 4, and 5. For this reason, we have verified that the retrieval of LST using three and five bands for the same date differs by approximately 0.03 K, which can be considered negligible for the aim of this work.

Once the input datasets were standardized and obtained with the procedure described above, the results were analyzed with the statistical indices reported as follows.

The Pearson correlation coefficient measures the linear correlation between two variables, regardless of scaling factors and offsets. Considering that a value greater than 0.7 indicates a high correlation, all the temperature fields derived from different sensors have a very good correlation. The highest correlations were obtained for Vesuvio and Mt. Etna areas, at 0.86 and 0.89, respectively (Table 4); the lowest correlation (0.66) was at the Solfatara area for the acquisition on 27 February 2019.

The bias parameter indicates the mean deviation between different temperature fields providing global information on under/overestimates. The bias values range from −2.47 K (Stromboli area) to +0.63 K (Vesuvio area), showing a great underestimation at Stromboli.

The RMSE parameter measures the spread between the different satellite images and estimates the goodness of fit; the resulting RMSE values are in the range 0.93–4.17 K, with the best agreement at the Vulcano area.

Summarizing the statistical results, we obtained the highest correlations at the Vulcano and Parco delle Biancane areas, with a slight overestimation from ECOSTRESS data (about +0.31 K) and very little spread (about 0.93 K). The worst fit is found for the Mt. Etna and Stromboli areas; for the latter area, temperatures are underestimated by ECOSTRESS (-2.47 K) and have a great spread (4.17 K). Regarding the comparison for the Stromboli area, the range of temperature values is the largest (290–390 K) due to the higher values linked to the volcanic eruption event. In this case, the higher values statistically lead to a remarkable difference (underestimation) in terms of absolute values. Instead, other greater over/underestimations occur for Vesuvio and Mt. Etna areas; these result from scatter plots (see Figure 4), and point distributions are prevalent in the upper-left sector and lower-right sector, respectively, for the Vesuvio and Mt. Etna cases.

Concerning the Solfatara areas, the comparison with ASTER data (Figures 3 and 5) shows a clear underestimation when using ECOSTRESS data; this observation could be due to the difference of acquisition time (about 50 minutes) during the night time due to the cooling phase of the soil.

The different acquisitions of these sensors, although similar, are not identical and can produce appreciable differences in the retrieved LSTs.

5. Conclusions

We used three different type of satellite data sets and two methodologies to obtain the LSTs of the main Italian active volcanoes and in an area with prominent geothermal activity. We found that LSTs retrieved using the two different methods and three sensors converged, in view of the high value correlation coefficient and the two normalized indices (bias and standard error). This comparison of surface temperatures derived from ECOSTRESS, L8 and ASTER shows that the new ECOSTRESS instrument is very compatible with the existing TIR instruments. ASTER is one of the more versatile satellite imagers used for studies of thermal anomalies; it can estimate surface temperatures with several thermal infrared spectral channels. TIRS-L8 images, while having fewer spectral channels and slightly lower spatial resolution than ASTER, provide additional temperature data for estimating and monitoring LST on active volcanoes as well as geothermal areas. ECOSTRESS's thermal infrared imager has the same number of channels as ASTER and a higher spatial resolution than ASTER or L8, plus a shorter revisit time. The additional ECOSTRESS data enable the increased monitoring of thermal anomalies compared to what is possible with ASTER and Landsat alone. With its shorter revisit time compared with ASTER and L8, ECOSTRESS represents a significant improvement in terms of the temporal sampling of LST.

References

1. Gianelli, G.; Ueckermann, H.I. A comparative analysis of the geothermal fields of Larderello and Mt. Amiata, Italy. *Geotherm. Energy Res. Trend* **2008**, *3*, 59–85.
2. Silvestri, M.; Rabuffi, F.; Pisciotta, A.; Musacchio, M.; Diliberto, I.S.; Spinetti, C.; Lombardo, V.; Colini, L.; Buongiorno, M.F. Analysis of Thermal Anomalies in Volcanic Areas Using Multiscale and Multitemporal Monitoring: Vulcano Island Test Case. *Remote Sens.* **2019**, *11*, 134. [CrossRef]
3. Silvestri, M.; Cardellini, C.; Chiodini, G.; Buongiorno, M.F. Satellite-derived surface temperature and in situ measurement at Solfatara of Pozzuoli (Naples, Italy). *Geochem. Geophys. Geosyst.* **2016**, *17*, 2095–2109. [CrossRef]
4. Chiodini, G.; Avino, R.; Caliro, S.; Minopoli, C. Temperature and pressure gas geoindicators at the Solfatara fumaroles (Campi Flegrei). *Ann. Geophys.* **2011**, *54*, 151–160. [CrossRef]
5. Buongiorno, M.F.; Pieri, D.; Silvestri, M. Thermal Analysis of Volcanoes Based on 10 Years of ASTER Data on Mt. Etna. *Therm. Infrared Remote Sens. Remote Sens. Digit. Image Process.* **2013**, *17*, 409–428.
6. Wright, R.; Flynn, L.P.; Garbeil, H.; Harris, A.J.; Pilger, E. MODVOLC: Near-real-time thermal monitoring of global volcanism. *J. Volcanol. Geotherm. Res.* **2004**, *135*, 29–49. [CrossRef]
7. Fujisada, H.; Sakuma, F.; Ono, A.; Kudoh, M. Design and preflight performance of ASTER instrument protoflight model. *IEEE Trans. Geosci. Remote Sens.* **1998**, *36*, 1152–1160. [CrossRef]
8. Yamaguchi, Y.; Kahle, A.; Tsu, H.; Kawakami, T.; Pniel, M. Overview of Advanced Spaceborne Thermal Emission and Reflection Radiometer (ASTER). *IEEE Trans. Geosci. Remote Sens.* **1998**, *36*, 1062–1071. [CrossRef]
9. Landsat 8. Available online: https://landsat.gsfc.nasa.gov/landsat-8/ (accessed on 28 October 2019).

10. Roy, D.P.; Wulder, M.A.; Loveland, T.R.; Woodcock, C.E.; Allen, R.G.; Anderson, M.C.; Zhu, Z. Landsat-8: Science and product vision for terrestrial global change research. *Remote Sens. Environ.* **2014**, *145*, 154–172. [CrossRef]

11. Barsi, J.; Schott, J.; Hook, S.; Raqueno, N.; Markham, B.; Radocinski, R. Landsat-8 thermal infrared sensor (TIRS) vicarious radiometric calibration. *Remote Sens.* **2014**, *6*, 11607–11626. [CrossRef]

12. Fisher, J.B.; Hook, S.; Allen, R.; Anderson, M.; French, A.; Hain, C.; Hulley, G.; Wood, E. The ECOsystem Spaceborne Thermal Radiometer Experiment on Space Station (ECOSTRESS): Science motivation. In Proceedings of the American Geophysical Union (AGU) Fall Meeting, San Francisco, CA, USA, 15–19 December 2014.

13. Fisher, J.B.; Hook, S.; Allen, R.; Anderson, M.; French, A.; Hain, C.; Hulley, G.; Wood, E. ECOSTRESS: NASA's next-generation mission to measure evapotranspiration from the International Space Station. In Proceedings of the American Geophysical Union (AGU) Fall Meeting, San Francisco, CA, USA, 14–18 December 2015.

14. ECOSTRESS. Available online: https://ecostress.jpl.nasa.gov/ (accessed on 28 October 2019).

15. ECOSTRESS Product Description. Available online: https://lpdaac.usgs.gov/products/eco1bmapradv001/ (accessed on 28 October 2019).

16. Berk, A.; Bernsten, L.S.; Robertson, D.C. *MODTRAN: A Moderate Resolution Model for LOWTRAN7*; GL-TR-89-0122; Air Force Geophysics Laboratory: Hanscom AFB, MA, USA, 1989.

17. Musacchio, M.; Amici, S.; Silvestri, M.; Teggi, S.; Buongiorno, M.F.; Silenzi, S.; Devoti, S. Application of CIRILLO: A new atmospheric correction tool on Castel Porziano Beach (CPB). *Remote Sens. Environ. Monit. GIS Appl. Geol. VII* **2007**, 674935. [CrossRef]

18. Sabol, D.E.; Gillespie, A.R.; Abbott, E.; Yamada, G. Field validation of the ASTER Temperature-Emissivity Separation algorithm. *Remote Sens. Environ.* **2009**, *113*, 2328–2344. [CrossRef]

19. Jiménez-muñoz, J.C.; Sobrino, J.A.; Mattar, C.; Hulley, G.; Göttsche, F. Temperature and Emissivity Separation from MSG/SEVIRI Data. *IEEE Trans. Geosci. Remote Sens.* **2013**, *52*, 1–15. [CrossRef]

20. Coll, C.; García-Santos, V.; Niclòs, R.; Caselles, V. Test of the MODIS Land Surface Temperature and Emissivity Separation Algorithm with ground measurements over a rice paddy. *IEEE Trans. Geosci. Remote Sens.* **2016**, *54*, 3061–3069. [CrossRef]

21. Gillespie, A.; Rokugawa, S.; Matsunaga, T.; Cothern, J.S.; Hook, S.; Kahle, A.B. A temperature and emissivity separation algorithm for Advanced Spaceborne Thermal Emission and Reflection Radiometer (ASTER) images. *IEEE Trans. Geosci. Remote Sens.* **1998**, *36*, 1113–1126. [CrossRef]

22. Hulley, G.C.; Hook, S.J. The North American ASTER Land Surface Emissivity Database (NAALSED) Version 2.0. *Remote Sens. Environ.* **2009**, *113*, 1967–1975. [CrossRef]

23. Islam, T.; Hulley, G.; Malakar, N.; Radocinski, R.; Guillevic, P.; Hook, S. A physics-based algorithm for the simultaneous retrieval of land surface temperature and emissivity from VIIRS thermal infrared data. *IEEE Trans. Geosci. Remote Sens.* **2017**, *55*, 563–576. [CrossRef]

24. Caputo, T.; Bellucci Sessa, E.; Silvestri, M.; Buongiorno, M.F.; Musacchio, M.; Sansivero, F.; Vilardo, G. Surface temperature multiscale monitoring by thermal infrared satellite and ground images at Campi Flegrei volcanic area (Italy). *Remote Sens.* **2019**, *11*, 1007. [CrossRef]

25. Il Parossismo dello Stromboli del 3 Luglio 2019 e L'attività nei Giorni Successivi: Il Punto Della Situazione al 13 Luglio 2019. Available online: https://ingvvulcani.wordpress.com/2019/07/13/il-parossismo-dello-stromboli-del-3-luglio-2019-e-lattivita-nei-giorni-successivi-il-punto-della-situazione-al-13-luglio-2019/ (accessed on 28 October 2019).

26. INGV Report. Available online: http://www.ct.ingv.it/it/rapporti/multidisciplinari.html (accessed on 28 October 2019).

27. Ecostress Data Description. Available online: https://ecostress.jpl.nasa.gov/downloads/20181017_ECOSTRESS_data_description-Frequently_Asked_Questions.pdf (accessed on 16 December 2019).